

# Magnetic switching modes for exchange spring systems $\text{ErFe}_2/\text{YFe}_2/\text{DyFe}_2/\text{YFe}_2$ with competing anisotropies

Jürgen P. Zimmermann,<sup>1</sup> Kevin Martin,<sup>2</sup> Giuliano Bordignon,<sup>1</sup> Matteo Franchin,<sup>1</sup>  
Roger C. C. Ward,<sup>3</sup> Graham J. Bowden,<sup>2</sup> Peter A. J. de Groot,<sup>2</sup> and Hans Fangohr<sup>1</sup>

<sup>1</sup> *Computational Engineering and Design Group, School of Engineering Sciences,  
University of Southampton, SO17 1BJ, United Kingdom*

<sup>2</sup> *School of Physics and Astronomy, University of Southampton, SO17 1BJ, United Kingdom*

<sup>3</sup> *Clarendon Laboratory, Oxford University, OX1 3PU, United Kingdom*

(Dated: December 12, 2008)

The magnetization reversal processes of  $[10\text{nmErFe}_2/n\text{YFe}_2/4\text{nmDyFe}_2/n\text{YFe}_2]$  multilayer films with a (110) growth axis and a variable  $\text{YFe}_2$  layer thickness  $n$  are investigated. The magnetically soft  $\text{YFe}_2$  compound acts as a separator between the hard rare earth (RE)  $\text{ErFe}_2$  and  $\text{DyFe}_2$  compounds, each of them bearing different temperature dependent magnetic anisotropy properties. Magnetic measurements of a system with  $n = 20\text{nm}$  reveal the existence of three switching modes: an independent switching mode at low temperatures, an  $\text{ErFe}_2$  spin flop switching mode at medium high temperatures, and an  $\text{YFe}_2$  dominated switching mode at high temperatures. The measurements are in qualitative agreement with the findings of micromagnetic simulations which are used to illustrate the switching modes. Further simulations for a varied  $\text{YFe}_2$  layer thickness  $n$  ranging from 2 nm to 40 nm are carried out. Quantitative criteria are defined to classify the reversal behavior, and the resultant switching modes are laid out in a map with regard to  $n$  and the temperature  $T$ . A new coupled switching mode emerges above a threshold temperature for samples with thin  $\text{YFe}_2$  separation layers as a consequence of the exchange coupling between the magnetically hard  $\text{ErFe}_2$  and  $\text{DyFe}_2$  layers. It reflects the increasing competition of the two conflicting anisotropies to dominate the magnetic switching states of both RE compounds under decreasing  $n$ .

## I. INTRODUCTION

Exchange spring magnets attract attention as potential candidates for a set of different applications. Firstly, there is the development of hard disks with ultra high storage densities: Ando and Nishihara implemented an exchange spring triple layer for perpendicular recording media in order to achieve a high signal-noise ratio and signal stability.<sup>1</sup> Victora and Shen suggested the usage of exchange spring multilayers as perpendicular magnetic recording media in order to facilitate the fabrication and to improve magnetic switching properties.<sup>2</sup> Suess *et al.* showed that the thermal stability of exchange spring recording media can be improved without increasing the coercive field, which is limited by the maximum field of the write head of roughly 1.7 T.<sup>3,4</sup> For thermally assisted magnetic recording (TAR), Thiele *et al.* used exchange spring media to allow for easier writing under a reduced coercive field above a transition temperature.<sup>5</sup>

The ongoing miniaturization of microelectromechanical systems (MEMS) promotes the development of magnetic MEMS (MagMEMS) devices as microsensors and microactuators, since magnetostatic interactions dominate over electrostatic effects on a nanometer scale. Several topical reviews exist.<sup>6-8</sup> Coils are economically and technically not viable as a magnetic flux generator in MagMEMS. Instead, exchange spring magnets, when tailored for a giant energy product and magnetic hardness,<sup>9-11</sup> could create high displacement rates in actuators, or high signal output in sensors, respectively.

In the field of spintronics, Kiselev *et al.*<sup>12</sup> and Xi *et al.*<sup>13</sup> reported on magnetic motions in a nanomag-

net driven by a spin-polarized current, possibly serving as an easily tunable nanoscale microwave generator. With their well defined interlayer domain walls stretching over vast parts of the multilayer, exchange springs are highly suitable for such devices, providing high spin torque yields. Furthermore, the spin torque emerges useful in order to manipulate switching states at comparably small applied fields.<sup>14</sup>

The utilization of exchange spring systems for the given applications requires a sound understanding of the switching processes and the magnetic spin configurations involved. These, in turn, depend on a set of parameters — the materials of the multilayer compounds with their respective anisotropy, saturation magnetization and exchange constants, the layer geometry and thickness, the temperature, and the applied field direction and field sweep range — and can be customized to individual needs. Asti *et al.* derived magnetic phase diagrams in terms of layer thicknesses by calculating the differential susceptibility at a nucleation field. In their one-dimensional models, uniaxial anisotropies were assumed with easy axes either in<sup>15</sup> or perpendicular to<sup>16</sup> the film plane.

In this paper, we focus on the magnetization reversal processes in  $[10\text{nmErFe}_2/n\text{YFe}_2/4\text{nmDyFe}_2/n\text{YFe}_2]$  multilayered exchange spring systems. These Laves phase superlattices can be epitaxially grown in a well-controlled and reproducible way, facilitating the production of samples with varied layer thickness  $n$ , but otherwise epitaxially identical. The two rare earth compounds,  $\text{ErFe}_2$  and  $\text{DyFe}_2$ , are among the materials with the highest magnetic anisotropies. In contrast, the  $\text{YFe}_2$  com-

pound bears negligible magnetic anisotropy. The Fe in either of the  $\text{YFe}_2$ ,  $\text{ErFe}_2$ ,  $\text{DyFe}_2$  compounds is responsible for the exchange interaction within and across the layers, and the exchange stiffness is widely homogeneous throughout the sample. Consequently, the ratio of the layer thicknesses of hard and soft compounds represents a parameter which allows us to tune the impact of the RE anisotropy on the magnetic switching states independent of intricacies imposed by the exchange interaction.

A further interesting aspect of the investigated system is the pre-strung magnetization configuration of the soft  $\text{YFe}_2$  compound: since the  $\text{YFe}_2$  layers are sandwiched between two different magnetically hard layers  $\text{ErFe}_2$  and  $\text{DyFe}_2$  with differing anisotropy properties, a domain wall is present in the intermediate  $\text{YFe}_2$  layer even in the remanent state. This is different to simpler systems with only one hard compound, where the magnetization in the soft compound is completely relaxed in the remanence state.

In the following, we present magnetization measurements along the  $[110]$  direction of a sample with  $n = 20$  nm for a set of temperatures  $T$  between 10 K and 300 K. They are compared to the results of micromagnetic simulations with OOMMF<sup>17</sup>, and the observed switching modes with their respective spin configurations are explained on the basis of the simulation data. Next, the thickness layer  $n$  is varied: graphs of the direction cosines of the compound specific magnetizations suggest a quantifiable definition of the switching modes. The switching modes are analyzed and their regimes are mapped with regard to  $T$  and  $n$ . The limiting curves of the regimes are understood by energy considerations.

## II. METHOD

### A. Numerical model

We use the OOMMF code<sup>17</sup> for our simulations, with extensions for higher order anisotropy energy terms.<sup>18</sup> For the time evolution, the Landau-Lifschitz-Gilbert equation is employed, determining quasi-static magnetization configuration states by a damped precession of the magnetization.

For the underlying numerical model, we assume a homogeneous magnetization in the  $(110)$  film plane, allowing us to represent the system by a 1d chain of computational cells along  $[110]$ . The computational cell size of  $1 \text{ nm}^3$  is sufficiently smaller than the exchange length of either compound material. We further draw on the ferromagnetism of the  $\text{ReFe}_2$  materials and assume a rigid exchange coupling of the magnetic moments of the 8 RE and the 16 iron atoms inside a lattice cell (FIG. 1): neighboring atoms of the same element couple ferromagnetically (RE-RE and RE-Fe), neighboring atoms of different elements couple antiferromagnetically (RE-Fe). Thus, we can calculate an effective magnetic moment  $\mathbf{m}_{\text{eff}}$  of a crystal cell by a simple signed summation of the con-

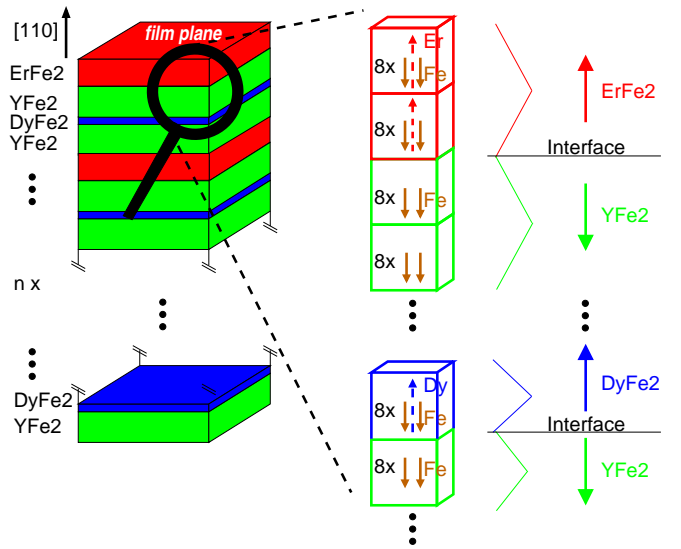


FIG. 1: (Color) Sketch of the underlying numerical model, showing the layers of  $\text{ErFe}_2/\text{YFe}_2/\text{DyFe}_2/\text{YFe}_2$  compounds (left), and the rigid coupling of the atomic moments to an effective magnetization for each compound (right). The arrows representing the atomic moments reflect the relative antiferromagnetic alignment of RE and Fe inside a crystal cell and the relative ferromagnetic alignment of Fe across the cells, not the real magnetization directions.

stituent moments inside. As the magnetic moments of Er and Dy outweigh that of Fe by at least a factor of 2, the effective moments of  $\text{ErFe}_2$  and  $\text{DyFe}_2$  oppose the moment of the atomic Fe. The magnetic moment of Y is negligible, and the only contribution to  $\mathbf{m}_{\text{eff}}(\text{YFe}_2)$  is the Fe moment. Across crystal cells, we only consider the ferromagnetic coupling of the Fe atoms. This results in a positive intra-layer exchange coupling  $A_{\text{intra}}$  for all compounds, a negative across-layer exchange coupling  $A_{\text{across}(\text{RE-Y})}$  between the effective  $\text{ReFe}_2$  and  $\text{YFe}_2$  moments, and a positive across-layer exchange coupling  $A_{\text{across}(\text{RE-RE})}$  between the effective  $\text{ErFe}_2$  and  $\text{DyFe}_2$  moments. The approximation of the demagnetizing energy density

$$\epsilon_{d,i} = \frac{1}{2} \mu_0 \mathbf{M}_i^2 \quad (1)$$

is valid under the condition of homogeneously magnetized thin film slabs  $i$  with a magnetization  $\mathbf{M}_i$ .

### B. Material parameters

We use the exchange constants  $A_{\text{intra}} = A_{\text{across}(\text{RE-RE})} = -A_{\text{across}(\text{RE-Y})} = 1.46 \times 10^{-11} \text{ J/m}$ . Ab initio calculations yield the temperature dependent atomic magnetic moments of Er, Dy, and Fe needed to assemble the effective magnetic moments as described in II A, and the saturation magnetization for the compounds is achieved by taking into account the cell sizes

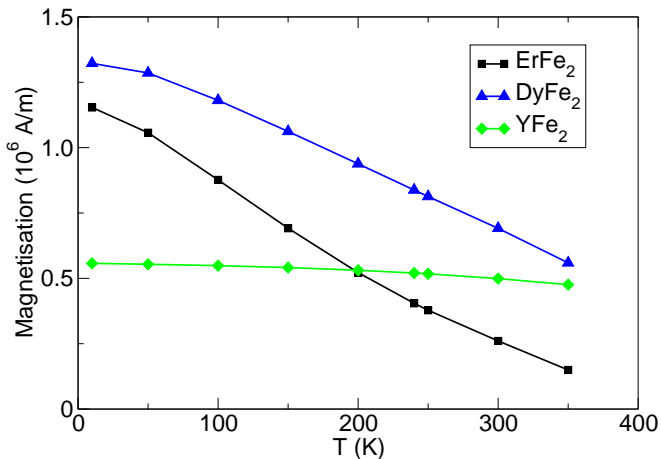


FIG. 2: (Color) Effective magnetization of ErFe<sub>2</sub> (black squares), DyFe<sub>2</sub> (blue triangles), and YFe<sub>2</sub> (green diamonds) as a function of temperature.

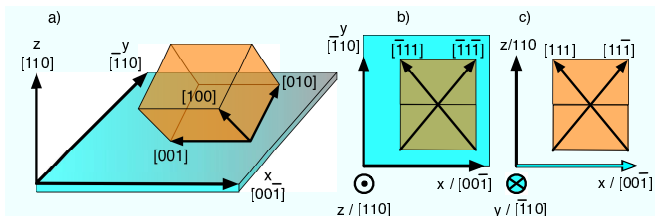


FIG. 3: (Color) (a) Lattice cell (yellow cube) with respect to the film plane (blue). The lab system is spanned by the basis vectors  $\mathbf{x}$ ,  $\mathbf{y}$ ,  $\mathbf{z}$ , the lattice cell by  $[100]$ ,  $[010]$ ,  $[001]$ . The crystal is grown in the  $[110]$  direction. (b) In-film-plane body diagonals of the lattice cell in an  $xy$  cross section (c), out-of-film-plane body diagonals in an  $xz$  cross section.

0.728 nm/0.732 nm/0.736 nm for ErFe<sub>2</sub>/DyFe<sub>2</sub>/YFe<sub>2</sub>.<sup>19</sup> The result can be seen in FIG. 2: For low temperatures  $\lesssim 200$  K, DyFe<sub>2</sub> and ErFe<sub>2</sub> magnetizations prevail, whereas for temperatures  $\gtrsim 200$  K YFe<sub>2</sub> starts dominating over ErFe<sub>2</sub> and increasingly catches up with DyFe<sub>2</sub>. For all temperatures considered, the magnetization of DyFe<sub>2</sub> exceeds that of ErFe<sub>2</sub>.

The orientation of the lattice cell with its basis vectors  $[001]$ ,  $[010]$ ,  $[001]$  in the lab system  $x, y, z$  for the crystal growth direction  $[110]$  are outlined in FIG. 3. The RE magnetocrystalline (MC) anisotropy of the bulk is described by the phenomenological parameters  $K_1$ ,  $K_2$ ,  $K_3$  of a cubic anisotropy energy density

$$\epsilon_{\text{MC}} = K_1 [\alpha_{100}^2 \alpha_{010}^2 + \alpha_{100}^2 \alpha_{001}^2 + \alpha_{010}^2 \alpha_{001}^2] + K_2 [\alpha_{100}^4 \alpha_{010}^2 \alpha_{001}^2 + \alpha_{100}^4 \alpha_{010}^2 \alpha_{001}^2] + K_3 [\alpha_{100}^4 \alpha_{010}^4 + \alpha_{100}^4 \alpha_{001}^4 + \alpha_{010}^4 \alpha_{001}^4], \quad (2)$$

where  $\alpha_{100}$ ,  $\alpha_{010}$ ,  $\alpha_{001}$  are the direction cosines of the magnetization with respect to the crystal lattice  $[100]$ ,  $[010]$ , and  $[001]$  directions. The  $K_1$ ,  $K_2$ ,  $K_3$  values

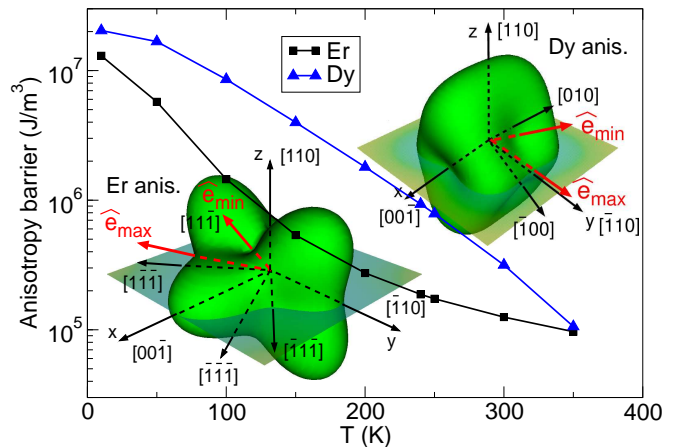


FIG. 4: (Color) Anisotropy energy barriers of Er (black squares) and Dy (blue triangles) as a function of temperature. The energy barrier is the anisotropy difference with regard to a maximum direction ( $\hat{\mathbf{e}}_{\text{max}}$ ) and a minimum direction ( $\hat{\mathbf{e}}_{\text{min}}$ ), as depicted in the insets in the lower left corner (Er) and upper right corner (Dy).

are taken from calculations extending the Callen-Callen model to second order.<sup>20</sup>

Additionally, a shear strain  $\epsilon_{xy}$  is present due to the  $[110]$  MBE growth direction of the films,<sup>21</sup> incorporated in the strain energy density

$$\epsilon_S = b_2 \epsilon_{xy} \alpha_x \alpha_y, \quad (3)$$

with the temperature dependent magnetoelastic constant  $b_2$ . The  $\alpha_x$ ,  $\alpha_y$ ,  $\alpha_z$  are direction cosines of the magnetization with respect to the basis vectors of the lab system. The term can be approximated by the first-order Callen-Callen term  $\tilde{K}'_2$  as

$$\epsilon_S = \tilde{K}'_2 [\alpha_z^2 - \alpha_y^2], \quad (4)$$

the values of which are given in Bowden *et al.*<sup>22</sup> The energy term (4) is a superposition of two uniaxial anisotropies of identical weight, one with a symmetry axis in  $z$ , the other in  $y$  with opposite sign. The strain term generally attenuates slower with rising temperature as the MC contribution. Consequently, the total anisotropy as a sum of MC anisotropy and strain term shows temperature dependent characteristics (find visualization of crystal directions in insets of FIG. 4 and in FIG 3): ErFe<sub>2</sub> has easy magnetization directions along the body diagonals of the lattice cell  $\langle 11\bar{1} \rangle$  for low temperatures (i.e. 10 K). For increasing temperatures, the out-of-plane easy axes move from  $[111]$  /  $[\bar{1}\bar{1}\bar{1}]$  towards  $[110]$ , the in-plane easy axes from  $[\bar{1}\bar{1}\bar{1}]$  /  $[\bar{1}\bar{1}\bar{1}]$  towards  $[001]$  due to the strain term becoming more pronounced. For DyFe<sub>2</sub>, the out-of-plane easy axes gradually rotate from  $[\bar{1}00]$  /  $[010]$  towards  $[\bar{1}10]$  under rising temperature, and the  $[001]$  easy axis eventually turns into a hard axis. Zhukov *et al.*<sup>23</sup> stated an out-of-plane angle of the

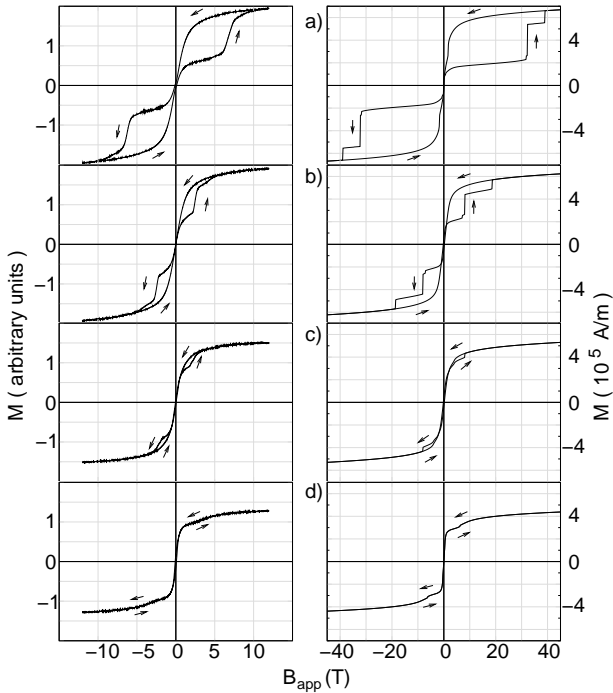


FIG. 5: Overall magnetization curves as a result of measurements (left column) and simulations (right column) for different temperatures with a separation layer thickness 20 nm. The temperatures are 10 K (exp.) / 10 K (sim.) (a), 95 K (exp.) / 100 K (sim.) (b), 200 K (exp.) / 200 K (sim.) (c), 290 K (exp.) / 300 K (sim.) (d). The arrows indicate the sweep direction of the applied field.

easy directions  $\theta \approx 14^\circ$  at 290 K. For our simulations, we adjust the DyFe<sub>2</sub> anisotropy parameters to take this into account: the  $\tilde{K}'_2$  of Bowden *et al.*<sup>22</sup> seems to underestimate the strain. This is apparent in an excessive  $\theta$  determined by simulations where the applied field in [110] is gradually relaxed, and the magnetization settles in the out-of-plane anisotropy minimum. After multiplying the  $\tilde{K}'_2$  values with a factor of 2.5 we are able to replicate the findings of Zhukov.<sup>23</sup>

We analytically determine the anisotropy energy barriers for Er and Dy most relevant in a demagnetizing process along the [110] direction (FIG. 4). Both barriers fade with rising temperature, facilitating switching processes.

The magnetization characteristics of specific DyFe<sub>2</sub>/YFe<sub>2</sub> and ErFe<sub>2</sub>/YFe<sub>2</sub> systems are described elsewhere.<sup>24–26</sup> We will now focus on generalized [10nmErFe<sub>2</sub>/*n*YFe<sub>2</sub>/4nmDyFe<sub>2</sub>/*n*YFe<sub>2</sub>] systems with different *n*, and start with *n* = 20 nm.

### III. EXPERIMENTAL DATA: THE *n* = 20nm SAMPLE

A [10nmErFe<sub>2</sub>/*n*YFe<sub>2</sub>/4nmDyFe<sub>2</sub>/*n*YFe<sub>2</sub>] superlattice with *n* = 20 nm is grown by molecular beam epitaxy

(MBE). The [110] growth direction of the Laves phase materials is in accordance with the strain term contribution to the anisotropy of the numerical model (eq. 3). The samples are magnetically characterized along the [110] direction by the use of a vibrating sample magnetometer (VSM).

The resulting hysteresis loops for the total magnetization are presented in the left column of Fig. 5 for four temperatures (a to d). For 10 K (5a) the loop features a typical exchange spring appearance insofar as the magnetization smoothly slopes when the applied field relaxes from a maximum positive value — the unwinding of the soft YFe<sub>2</sub> magnetization into a ferrimagnetic alignment. Whereas an exchange spring system with one magnetically hard material shows one step-down indicating the switching of the hard compound, here we see one larger drop at an applied field  $B_{S1}$  of around -6 T, and a smaller one at an applied field  $B_{S2}$  of around -8 T. It seems obvious to identify the former with the switching of the ErFe<sub>2</sub> compound into the applied field direction, the latter with that of DyFe<sub>2</sub>: in the case of DyFe<sub>2</sub>, higher anisotropy energy barriers have to be overcome before the switching takes place (FIG. 4). Furthermore, the different step amplitudes match the ratio of the RE layer thicknesses (4 nm:10 nm).

For 95 K (5b), the shape of the hysteresis loop is widely unchanged, but the switching fields are substantially decreased, with  $B_{S1}$  around -2.5 T and  $B_{S2}$  around -4 T. In the hysteresis loop for 200 K (5c), the large drop attributed to the ErFe<sub>2</sub> switching has disappeared, with only the small DyFe<sub>2</sub> switching step left at  $B_{S2}$  of -2 T. At 295 K (5d), the hysteresis loop presents a small kink at a field  $B_K$  of approximately -3 T with no notable coercivity. Otherwise, the curve is smooth.

For all four temperatures, there is no coercive field of relevance. This leaves us with three different types of appearance for the hysteresis loops of the *n* = 0 sample: A low temperature (LT) type for 10 K and 95 K, a medium temperature (MT) type for 200 K, and a high temperature (HT) type for 290 K.

### IV. MODELING OF HYSTERESIS LOOPS

In order to receive more insight into the detailed spin configurations, we run micromagnetic simulations based on the numerical model outlined in II. The applied field is swept along the [110] axis perpendicular to the film plane from +60 T to -60 T to +60 T with a resolution of 160 mT. First, hysteresis loops are generated in order to compare them to the measurements and to confirm the numerical model. The resulting hysteresis loops (10 K, 100 K, 200 K, 300 K) are placed next to the experimental loops with the same or very similar temperatures on the right column of FIG. 5. For all four temperatures, the shapes of the magnetization curves of the simulations bear a striking resemblance to those of the measurements, featuring all the characteristics described earlier. The

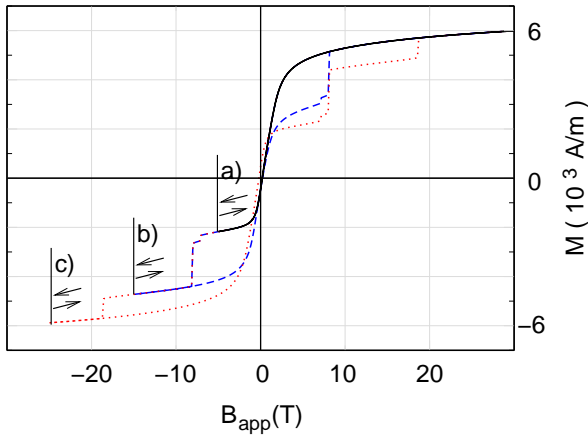


FIG. 6: (Color) Overall hysteresis loop for an  $\text{YFe}_2$  layer thickness of 20 nm at  $T=100$  K for different applied field sweeps. The applied field is varied from +30 T to -4.96 T (solid black line, a) / -14.88 T (dashed blue line, b) / -24.96 T (red dotted line, c) and back to +30 T to check the reversibility of the corresponding hysteresis loop parts.

switching fields, however, are too large: for 10 K,  $B_{S1}$  is -32 T, and  $B_{S2}$  -39 T. For 100 K,  $B_{S1}$  is -8 T, and  $B_{S2}$  -18 T. We find a  $B_{S2}$  of -8 T for 200 K, and  $B_K$  of -6 T for 300 K. The values deviate roughly by a factor of 2 for 300 K and by a factor of 5 for 10 K. The excessive switching fields of the simulations are a consequence of the 1d model with its inability to nucleate, a fact known as Brown's paradox.<sup>27-29</sup> In spite of this inherent problem, the agreement of the simulation and measurement loops is formidable and justifies further interpretation of the numerical data.

The reversibility of selected sections of the hysteresis loop for a temperature of 100 K is elucidated in FIG. 6 in the case of the simulations: the applied field is swept to a specific target value just beyond the section of interest, and the field sweep direction is reversed. Irreversibilities are then recognizable when the curves for the two different sweep directions are not congruent. The two steps for negative applied fields turn out to be irreversible (FIG. 6bc), the exchange spring unwinding (FIG. 6a) to be reversible, underpinning the interpretation of the experimental hysteresis loops. The two hard compounds  $\text{ErFe}_2$  and  $\text{DyFe}_2$  switch independently of each other.

## V. MODELING OF SWITCHING MODES

We now explain the different magnetic reorientation processes underlying the LT, MT, HT appearances of the hysteresis loops. For this, we use the numerical data to determine the compound-specific magnetization curves: each numerical cell is represented by one magnetization vector, and for each of the  $\text{DyFe}_2$  /  $\text{ErFe}_2$  /  $\text{YFe}_2$  compounds separately, the magnetization vectors of the numerical cells for the respective layers are averaged. The

result is depicted in FIG. 7 for the domains of LT ( 100 K, 7a ), MT ( 200 K , 7b ), and HT ( 300 K and 350 K, 7cd ). Each of the four graphs shows the compound-specific magnetization curves on top. In the middle, the characteristic switching states for the specific  $\text{ErFe}_2$  and  $\text{DyFe}_2$  magnetization are visualized as 3d vectors on top of the anisotropy energy surfaces of Er and Dy. On the bottom, the Er and Dy anisotropy energies are plotted for the magnetization directions at the respective applied field.

For 100 K (FIG. 7a), the compound-specific magnetization loops confirm the presumed individual switching of the RE compounds and the exchange spring unwinding of the soft  $\text{YFe}_2$  compound. For positive applied fields ( $\Rightarrow$  state (1)), the RE moments are located in their respective anisotropy energy dips —  $\text{ErFe}_2$  at  $[11\bar{1}]$ ,  $\text{DyFe}_2$  at  $[010]$ . The  $\text{YFe}_2$  moments, antiferromagnetically coupled to the RE moments, oppose the applied field direction  $\mathbf{B}_{\text{app}}$  at the interfaces, and wind towards  $\mathbf{B}_{\text{app}}$  in the interior. At state (1), the majority of the  $\text{YFe}_2$  moments is aligned with the strong field, and its magnetization is positive. When the field abates, the  $\text{YFe}_2$  moments gradually unwind and their magnetization reverses at positive applied fields. In the remanent state, the  $\text{YFe}_2$  moments are antiferromagnetically aligned at the interfaces, towards  $[0\bar{1}0]$  at the  $\text{DyFe}_2$  side, and  $[\bar{1}\bar{1}1]$  at the  $\text{ErFe}_2$  side, and uniformly swerve in between. Under a field rising in the reversed direction, the RE moments are gradually dragged out of their anisotropy dips, recognizable from the ascent in the anisotropy energy plots of the compounds at the bottom of the graph.  $\text{ErFe}_2$  is the first to switch at -8 T ( $\Rightarrow$  state (2)), followed by  $\text{DyFe}_2$  at -18 T ( $\Rightarrow$  state (3)). Each time,  $\text{YFe}_2$  stays aligned with the applied field direction. Both switchings are accompanied by a sharp drop in the corresponding anisotropy energy. We define this the **independent switching mode**, referring to the independent RE switchings.

A new mode applies for 200 K (FIG. 7b);  $\text{ErFe}_2$  now reverses via the spin flop direction  $[\bar{1}\bar{1}\bar{1}]$ , embodied in the extra state (2). The  $\text{ErFe}_2$  moments rotate into the spin flop state at a positive applied field of around 3 T. The process can be understood by magnetic energy considerations: at high applied fields, both the majority of  $\text{YFe}_2$  moments and  $\text{ErFe}_2$  moments are aligned with the field direction, with a domain wall around their mutual interface. Exchange coupling tries to push one compound into an antiferromagnetic alignment, but is outbalanced by the large Zeeman energies. When the applied field is sufficiently reduced, the  $\text{YFe}_2$  moments at some point start to unwind. If beforehand the effect of the exchange interaction acting on  $\text{ErFe}_2$  exceeds the Zeeman energy of  $\text{ErFe}_2$  plus the Er anisotropy barrier, then the  $\text{ErFe}_2$  moments rotate against the applied field direction into the spin flop state. Whether this condition is fulfilled, depends on the temperature: for rising temperatures the magnetic moment of  $\text{ErFe}_2$  sharply decays (FIG. 2), and with it the corresponding Zeeman energy. Additionally, the Er anisotropy energy barrier degrades logarithmically

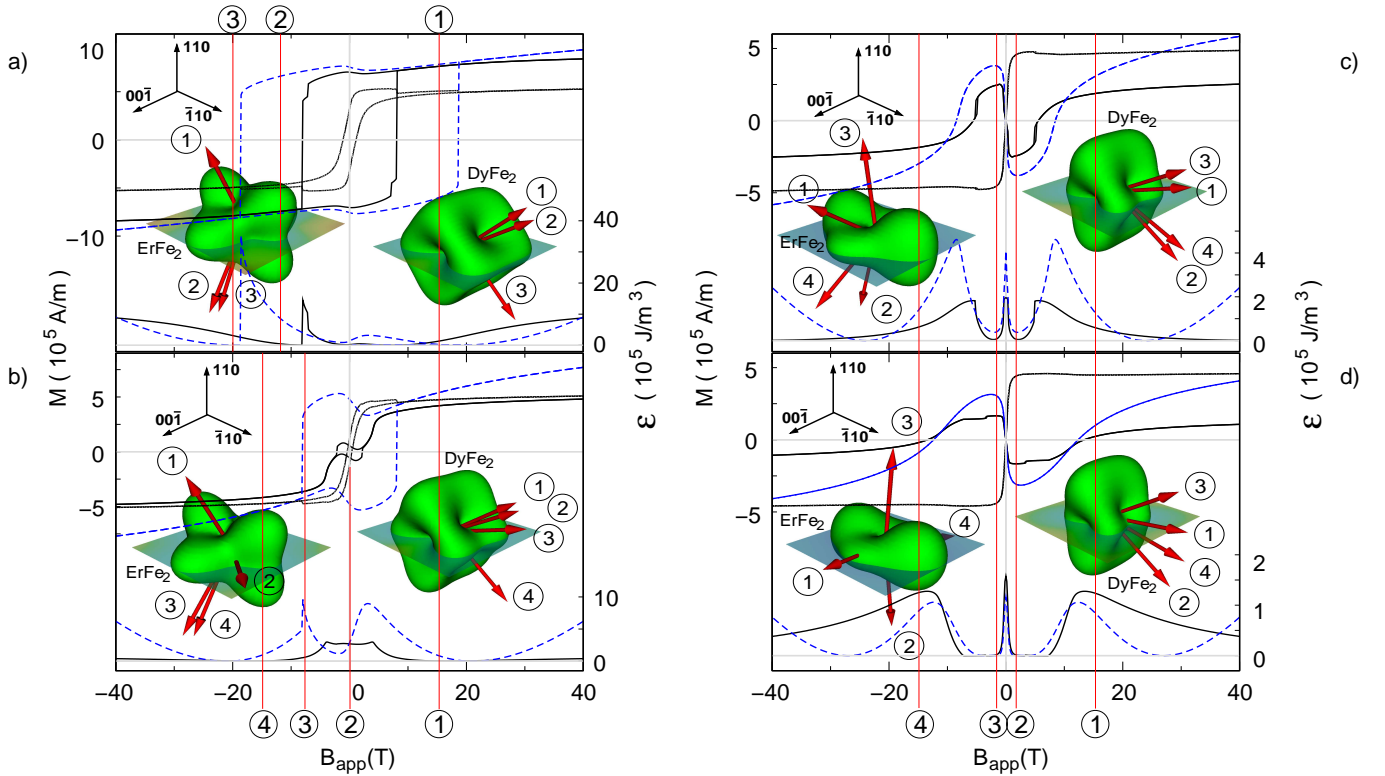


FIG. 7: (Color) Compound-specific magnetization curves and switching states for the temperatures 100 K (a), 200 K (b), 300 K (c), 350 K (d), and an  $\text{YFe}_2$  separation layer thickness 20 nm. In the upper section of each graph, the compound-specific magnetization curves in the direction of the applied field  $[110]$  (black solid line for  $\text{ErFe}_2$ , blue dashed line for  $\text{DyFe}_2$ , brown checkered line for  $\text{YFe}_2$ ) are shown as a result of the simulations. In the lower section of the graphs, the anisotropy energy densities for the RE compounds (same color coding) are depicted for the corresponding magnetization directions. In the insets, characteristic switching states are visualized ( $\text{ErFe}_2$  on the left,  $\text{DyFe}_2$  on the right): the magnetization of a compound is specified by a red arrow on the green anisotropy surface. Each state is labeled with a number referring to an applied field that is marked by a numbered red horizontal line. The crystallographic directions as an orientation for the anisotropy surfaces are set in the upper left corner of each graph.

(FIG. 4). Both effects together cause the energy condition to become true above a critical temperature  $T_{\text{crit,Er}}$ ; and a spin flop state is achieved for the  $\text{ErFe}_2$  moments. Analysis of the anisotropy energy function shows that there is a distinct minimum around  $[\bar{1}\bar{1}\bar{1}]$  for temperatures of 200K or lower, allowing the  $\text{ErFe}_2$  moments to settle in this direction. When the field is increased in the opposite direction to -3 T,  $\text{ErFe}_2$  is finally dragged out of the spin flop state into state (3) by Zeeman interaction. The  $\text{DyFe}_2$  magnetization stays in the  $[010]$  direction until it switches into state (4) /  $[0\bar{1}0]$  at -8 T. We define this the **ErFe<sub>2</sub> spin flop mode**.

Under a further increase of the temperature to 300 K (FIG. 7c), both  $\text{DyFe}_2$  (at 8 T) and  $\text{ErFe}_2$  (at 5 T) moments reverse for positive fields already ( $\Rightarrow$  state (2)). Whereas in the case of 200K, the  $\text{ErFe}_2$  moments reside in the spin flop state  $[\bar{1}\bar{1}\bar{1}]$ , they now rotate further into  $[\bar{1}\bar{1}\bar{1}]$ , off the applied field direction. The  $\text{YFe}_2$  magnetization stays pinned to the field direction, and both reverse together. Also the RE compounds switch ( $\Rightarrow$  state (3)) and stay in a direction opposing the ap-

plied field. Under a further decreasing applied field, the RE compounds switch a third time towards the applied field direction ( $\Rightarrow$  state (4)).

The reason why the  $\text{ErFe}_2$  moments do not settle in the spin flop direction is that the anisotropy energy surface of Er has changed for 300K due to the strain term, and the  $[\bar{1}\bar{1}\bar{1}]$  direction is now a saddle point. The new triple switching of  $\text{DyFe}_2$  can be explained by energy considerations similar to those for  $\text{ErFe}_2$  at 200K, but unlike that case, the anisotropy barrier obstructing access to the spin flop direction ( $[00\bar{1}]$  for  $\text{DyFe}_2$ ) stays impregnable, and it is energetically favorable for  $\text{DyFe}_2$  to reverse into  $[\bar{1}00]$  over the more viable  $[\bar{1}\bar{1}0]$  barrier. The critical temperature for the  $\text{DyFe}_2$  triple switching  $T_{\text{crit,Dy}}$  is higher than  $T_{\text{crit,Er}}$  because of the generally stronger Dy anisotropy. The spin flop mode is observed for  $T_{\text{crit,Er}} < T < T_{\text{crit,Dy}}$ , and for  $T > T_{\text{crit,Dy}}$  the **YFe<sub>2</sub> dominated switching mode** applies. It has to be emphasized that this mode is an extension of the  $\text{ErFe}_2$  spin flop mode in a way that the  $\text{ErFe}_2$  moments still transit the spin flop direction on their reversals.

A further example of the  $\text{YFe}_2$  dominated switching mode is given for 350K, with displaced  $\text{ErFe}_2$  spin directions: for high fields ( $\Rightarrow$  state (1)), the  $\text{ErFe}_2$  moments are not located around the Er anisotropy minimum any more, but close to  $[00\bar{1}]$  instead. Under the high temperature, the  $\text{YFe}_2$  magnetization has become so dominant under a vanishing Er anisotropy to be able to push the domain wall at the interface wide into the  $\text{ErFe}_2$  layer, thus keeping  $\text{ErFe}_2$  from rotating closer to the applied field and to its anisotropy minimum. In the states (2) and (3), the  $\text{ErFe}_2$  moments are largely pointing to the anti-field directions  $[\bar{1}10]$  and  $[110]$ ; a ferrimagnetic spin configuration with the prevailing  $\text{YFe}_2$ . Furthermore, these directions are now energetically favorable with regard to the Er anisotropy, due to the increased importance of the strain term contribution.

## VI. $\text{YFe}_2$ THICKNESS DEPENDENCE

So far, we have observed three switching modes for a sample with  $n = 20$  nm. The complex underlying re-orientation processes were interpreted by micromagnetic modeling. We now take this further and run simulations with a varied  $n$  in order to establish a map of switching modes. The corresponding parameter space is composed of a temperature range from 10 K to 400 K with a step resolution of 10 K, and a separation layer thickness range  $n \in \{2, 5, 7, 10, 12, 15, 17, 20, 22, 25, 27, 30, 32, 35, 37, 40\}$  nm.

### A. Identification of switching states

As we investigate a large number of magnetization curves, we require quantitative measures to efficiently identify magnetic switching states. The straightforward option is to analyze the compound-specific RE magnetizations, fixed by their direction cosines  $\alpha_{x,\text{RE}}$ ,  $\alpha_{y,\text{RE}}$ , and  $\alpha_{z,\text{RE}}$  with respect to the basis vectors  $[00\bar{1}]$ ,  $[\bar{1}10]$ , and  $[110]$  of the lab system. Per magnetization curve, the maxima  $\alpha_{x,\text{RE},\text{max}}$  and  $\alpha_{y,\text{RE},\text{max}}$  of each of the compound-specific direction cosines are determined — a measure for the range of the magnetization trajectories of the compounds. We focus on  $\alpha_{x,\text{RE},\text{max}}$  and  $\alpha_{y,\text{RE},\text{max}}$  as they provide suitable information about possible spin-flop configurations. Plots of these observables as a function of  $T$  for a selection of  $n$  are given in FIGS. 8 to 12.

In FIG. 8,  $\alpha_{x,\text{Er},\text{max}}$  is shown, where high values indicate a small deviation of the  $\text{ErFe}_2$  magnetization from the  $[00\bar{1}]$  direction, a hard axis of the Er anisotropy. The value at 10 K is around 0.8, independent of  $n$ . The huge anisotropy for very low temperatures is the sole crucial factor here to keep the  $\text{ErFe}_2$  moment  $\arccos 0.8 \approx 37^\circ$  off from  $[00\bar{1}]$ .

For medium high temperatures between 100 K and 250 K,  $\alpha_{x,\text{Er},\text{max}}$  generally drops, with a larger gradient for smaller  $n$ , and barely notable for  $n$  of 15 nm

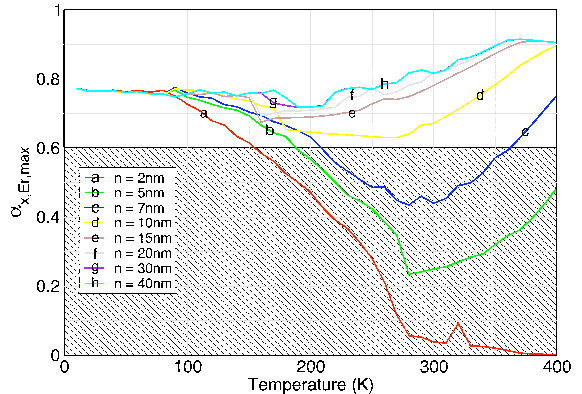


FIG. 8: (Color) Maximum direction cosine  $\alpha_{x,\text{Er},\text{max}}$  in  $[00\bar{1}]$  of the  $\text{ErFe}_2$  magnetization as a function of the temperature for different  $\text{YFe}_2$  layer thicknesses. The  $\text{YFe}_2$  layer thickness for each curve can be looked up in the legend. The hatched area indicates an  $\alpha_{x,\text{Er},\text{max}}$  smaller 0.6, signifying a distortion of the  $\text{ErFe}_2$  magnetization toward the  $\text{DyFe}_2$  moments.

or more. As the anisotropy decreases with temperature, the exchange interaction of the RE compounds becomes more important, amplified by a thinning of the  $\text{YFe}_2$  separation layer: the  $\text{ErFe}_2$  moments are attracted by the  $\text{DyFe}_2$  moments toward the  $(00\bar{1})$  plane perpendicular to the  $[00\bar{1}]$  direction.

For  $\alpha_{x,\text{Er},\text{max}}$  smaller than  $0.6 \approx \cos 57^\circ$ , the  $\text{ErFe}_2$  moments are distorted beyond the direction of its in-plane anisotropy minimum in  $\langle 11\bar{1} \rangle$ . We define this the **coupled switching mode**, as the  $\text{ErFe}_2$  moments are now significantly coupled to the  $\text{DyFe}_2$  moments. This mode is not observed in the  $n = 20$  nm sample investigated in section III due to the thick magnetic separation layer. An illustration is given in Fig. 9 for a  $n = 2$  nm sample: the exchange interaction between the RE compounds is strong enough to force the  $\text{ErFe}_2$  moments to reverse from state (2) to state (3) via the  $[\bar{1}10]$  direction that is unfavorable with regard to the Er anisotropy.

The maximum direction cosines of samples with  $n \geq 10$  nm converge to 0.9 for  $T$  reaching 400 K, and the  $n = 5/7$  nm samples show a sharp increase towards this value (unlike the  $n = 2$  nm sample). The reason for this high  $T$  behavior is the dominance of  $\text{YFe}_2$  under a diminishing Er anisotropy (discussed earlier in V) that causes  $\text{ErFe}_2$  to increasingly unwind toward the unfavorable  $[00\bar{1}]$  direction.  $\text{YFe}_2$  starts prevailing at lower  $T$  when its layer gets thicker. For  $n = 2$  nm, however,  $\text{YFe}_2$  never prevails, and  $\alpha_{x,\text{Er},\text{max}}$  stays around zero up to 400 K.

FIG. 10 pinpoints the spin flop states of the  $\text{ErFe}_2$  compound by depicting the maximum direction cosine  $\alpha_{x,\text{Er},\text{max}}$  of the  $\text{ErFe}_2$  magnetization with respect to  $[\bar{1}10]$ . Low values of  $\alpha_{x,\text{Er},\text{max}}$  correlate with  $\text{ErFe}_2$  moments staying in the  $(110)$  plane during the complete

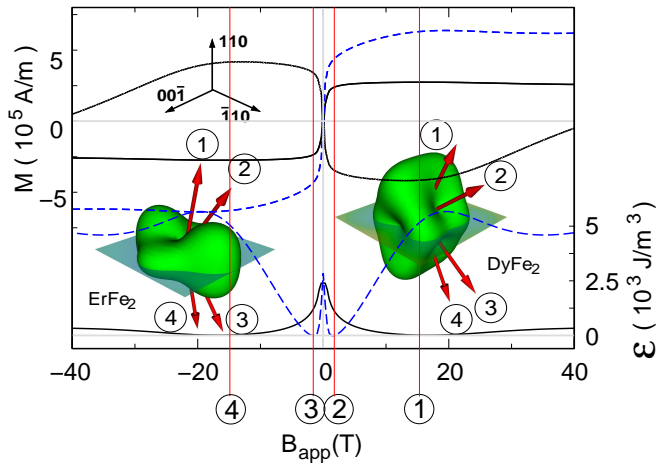


FIG. 9: (Color) Coupled switching mode: compound-specific magnetization curves and switching states for an  $\text{YFe}_2$  separation layer thicknesses of 2 nm and a temperature of 290 K. The explanation of the graphs follows FIG. 7.

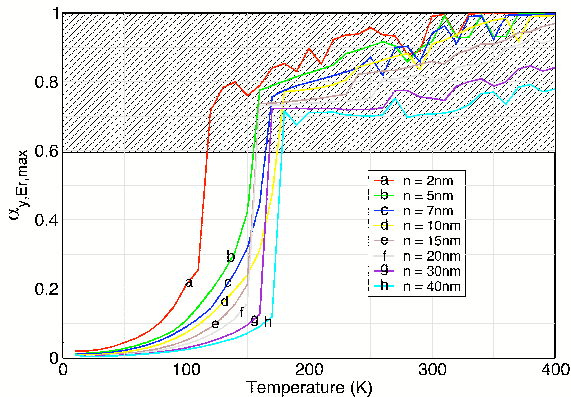


FIG. 10: (Color) Maximum direction cosine  $\alpha_{y,\text{Er,max}}$  in  $[\bar{1}10]$  of the  $\text{ErFe}_2$  magnetization as a function of the temperature for different  $\text{YFe}_2$  layer thicknesses. The  $\text{YFe}_2$  layer thickness for each curve can be looked up in the legend. The hatched area indicates an  $\alpha_{y,\text{Er,max}}$  larger 0.6, signifying spin flop directions of the  $\text{ErFe}_2$  magnetization.

magnetization cycle. High values suggest the existence of a spin flop state for at least one point in the hysteresis loop. For temperatures of less than 100 K, the  $\text{ErFe}_2$  moments of all samples clearly do not feature a spin flop state. However, when the temperature surpasses the critical value  $T_{\text{crit,Er}}$ , the  $\alpha_{x,\text{Er,max}}$  sharply ascend to values of over 0.6, marked by the hatched area in the graph, prevailing up to the maximum temperature of 400 K. This ledge confines the regime of the  $\text{ErFe}_2$  spin flop mode at the LT side, whereas the transition to the  $\text{YFe}_2$  dominated switching mode at the HT side still has to be

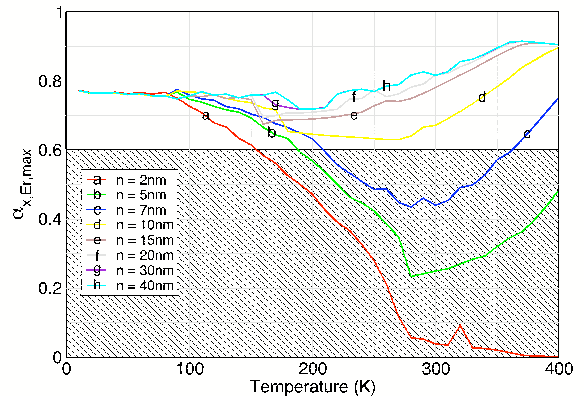


FIG. 11: (Color) Maximum direction cosine  $\alpha_{x,\text{Dy,max}}$  in  $[00\bar{1}]$  of the  $\text{DyFe}_2$  magnetization as a function of the temperature for different  $\text{YFe}_2$  layer thicknesses. The corresponding  $\text{YFe}_2$  layer thickness for each curve can be looked up in the legend. The hatched area indicates an  $\alpha_{x,\text{Dy,max}}$  larger 0.6, signifying spin flop directions of the  $\text{DyFe}_2$  magnetization.

laid out. Interestingly,  $T_{\text{crit,Er}}$  is considerably smaller for  $n = 2$  nm than for larger  $n$  values: the thin  $\text{YFe}_2$  separation layer cannot prevent the exchange interaction of the RE compounds; the  $\text{DyFe}_2$  moments attract the  $\text{ErFe}_2$  moments and facilitate  $\text{ErFe}_2$  to switch into the  $[\bar{1}1\bar{1}]$  spin flop state.

The occurrence of spin flop states for  $\text{DyFe}_2$  in the simulations follows from plots of the maximum direction cosine  $\alpha_{x,\text{Dy,max}}$  of the  $\text{DyFe}_2$  magnetization with respect to  $[00\bar{1}]$  in FIG. 11. The  $n = 2$  nm sample shows a solitary  **$\text{DyFe}_2$  spin flop mode** for  $T = 70$  K: the plot intrudes into the hatched area of magnetization directions that are elongated from  $[00\bar{1}]$  by more than  $57^\circ$ . Otherwise, no  $\text{DyFe}_2$  spin flop states are observed. The Dy anisotropy energy barrier separating the out-of-plane minimum from the in-plane spin-flop minimum is too high to be crossed — ignoring the one isolated exception.

Finally, FIG. 12 with its plots of the maximum direction cosine  $\alpha_{y,\text{Dy,max}}$  of the  $\text{DyFe}_2$  magnetization with respect to  $[\bar{1}10]$  suggests that the  $\text{DyFe}_2$  moments cannot be forced out of their natural  $(00\bar{1})$  plane by exchange coupling with  $\text{ErFe}_2$ . No plots intrude into the hatched area of the graph marking the range where the magnetization is considerably elongated towards  $[00\bar{1}]$ . As soon as relevant exchange interaction of the RE compounds emerges,  $\text{DyFe}_2$  takes control over  $\text{ErFe}_2$  (and not vice versa).

Finally, a numeric criterion is required to identify the  $\text{YFe}_2$  dominated switching mode. Following the definition of this mode in V, both RE compounds show a switching against the applied field direction. This is easily recognized for  $\text{DyFe}_2$  — a change of sign of the

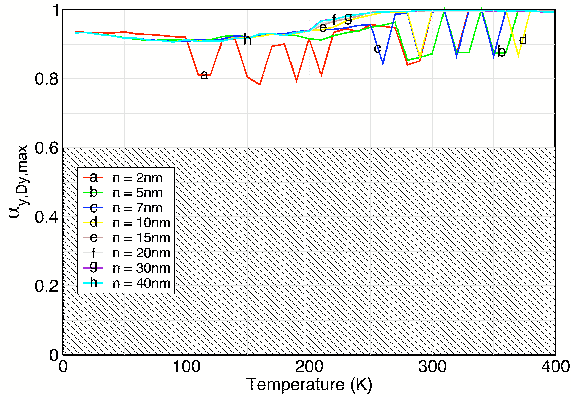


FIG. 12: (Color) Maximum direction cosine  $\alpha_{y,Dy,max}$  in  $[\bar{1}10]$  of the  $DyFe_2$  magnetization as a function of the temperature for different  $YFe_2$  layer thicknesses. The corresponding  $YFe_2$  layer thickness for each curve can be looked up in the legend. The hatched area indicates an  $\alpha_{y,Dy,max}$  smaller 0.6, signifying a distortion of the  $DyFe_2$  magnetization toward the  $ErFe_2$  moments.

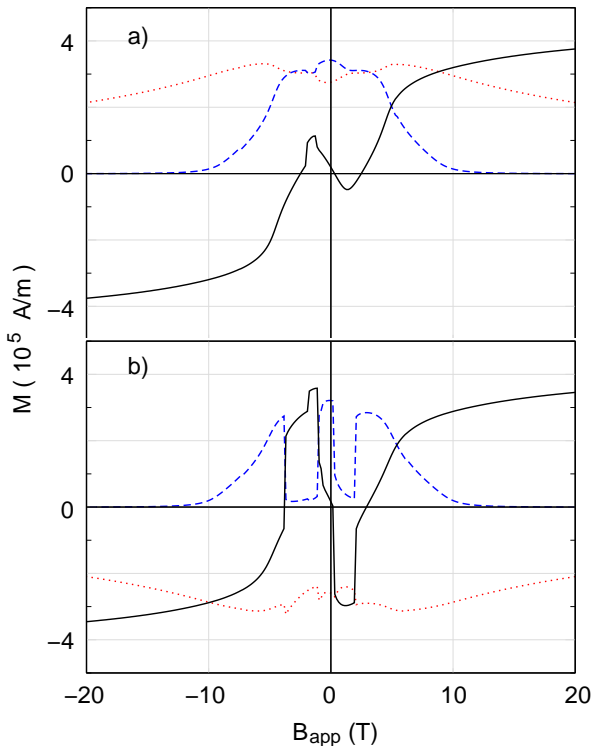


FIG. 13: (Color)  $ErFe_2$  magnetization components in  $[110]$  (black solid line) /  $[\bar{1}10]$  (blue dashed line) /  $[00\bar{1}]$  (red dotted line) direction for 220 K (a) and 230 K (b): the snapping of the  $ErFe_2$  magnetization in the case of 230 K is indicated by the drop of the  $[\bar{1}10]$  component for about 1.5 T applied field.

$[110]$  magnetization component for positive  $B_{app}$ . However, this condition is not sufficient in the case of  $ErFe_2$ : in the vicinity of the in-plane spin flop state  $[\bar{1}1\bar{1}]$ , the  $[110]$  magnetization component of  $ErFe_2$  can change sign without any switching. Looking at all three magnetization components of the  $ErFe_2$  compound in FIG. 13 for  $T = 220$  K (a,  $ErFe_2$  spin flop mode) and  $T = 230$  K (b,  $YFe_2$  dominated switching mode) provides us with an unambiguous  $ErFe_2$  switching criterion. While the  $[110]$  component changes sign at  $B_{app} \approx 2.5$  T for both 220 and 230 K, the  $[\bar{1}10]$  component drops only for  $T = 230$  K when the  $ErFe_2$  moments snap into the  $[\bar{1}1\bar{1}]$  direction. Thus, the magnetization decline in  $[110]$  in combination with the sign change in  $[\bar{1}10]$  marks the  $ErFe_2$  reversal against the applied field.

## B. Phase diagram

We can now map the regimes of different switching modes on a  $T/n$  landscape (FIG. 14). In a nutshell, the regime of the individual switching mode is at the LT side, the regime of the  $YFe_2$  dominance mode in the HT/high  $n$  corner, with the regime of the  $ErFe_2$  spin flop mode stretching between the two. The regime of the coupled switching mode is placed on the HT section of the low  $n$  edge. It is not an independent mode but rather an extension to one of the former modes. Thus, the coupled switching regime is superposed to either the  $ErFe_2$  spin flop regime or the  $YFe_2$  dominance regime. We ignore the solitary  $DyFe_2$  spin flop mode at 70 K for  $n = 2$  nm.

The divide between the independent switching regime and  $ErFe_2$  spin flop regime runs along a roughly vertical line with temperatures around 150 to 170 K for  $n > 2$  nm. The increasing mutual RE exchange coupling for low  $n$  assists the  $ErFe_2$  moments in reversing via the spin flop mode, and the  $ErFe_2$  spin flop regime stretches further out to 120 K for smallest  $YFe_2$  separation.

The conditions for the  $YFe_2$  dominance are a sufficiently high temperature in order to truncate the anisotropy barriers, and an adequately thick  $YFe_2$  layer to outweigh the RE compounds. Consistently, the regime is found in the high  $T$ /high  $n$  corner, in a segment-like area delimited to  $T = 220$  K for maximum  $n$ , and  $n = 5$  nm for maximum  $T$ .

The regime where the  $ErFe_2$  moments tend to couple to the  $DyFe_2$  moments is located in the low  $n$  area where the magnetic separation barely impedes the mutual RE exchange coupling. It extends to a peak  $n = 7$  nm between  $T = 210$  K and  $T = 360$  K. The decay of the Er anisotropy under a rising temperature facilitates the distortion of the  $ErFe_2$  by exchange coupling; this is reflected in the curved LT border of the coupled switching regime that extends further to  $T = 160$  K for  $n = 2$  nm, compared to  $T = 210$  K for  $n = 7$  nm.

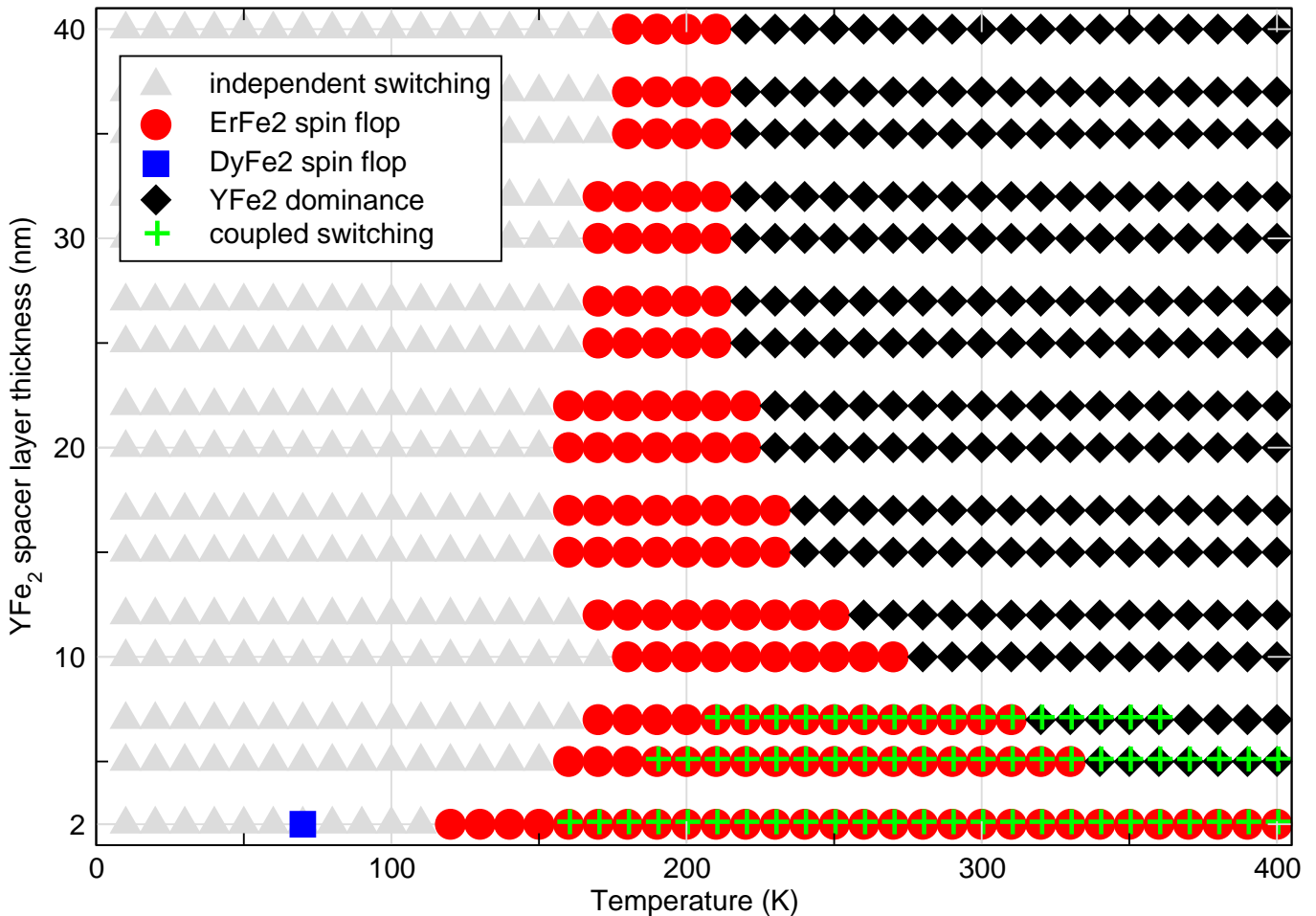


FIG. 14: (Color) Switching modes for different temperatures and YFe<sub>2</sub> separation layer thicknesses as a result of simulations using the numerical model given in FIG. 1. The grey triangles pointing up represent the independent switching mode, where the magnetizations of both RE compounds hysteretically switch into the direction of the applied field. The red circles indicate the ErFe<sub>2</sub> spin flop mode. The black diamonds signify the YFe<sub>2</sub> dominance mode with RE unwinding against the applied field direction. Superimposed green crosses refer to a distortion of the ErFe<sub>2</sub> moments toward the DyFe<sub>2</sub> switching plane (00 $\bar{1}$ ), the coupled switching mode. The solitary DyFe<sub>2</sub> spin flop state is denoted by a blue square.

## VII. CONCLUSION

Magnetic measurements of a [10nmErFe<sub>2</sub>/20nmYFe<sub>2</sub>/4nmDyFe<sub>2</sub>/20nmYFe<sub>2</sub>] system indicate the existence of three different switching modes over a temperature range from 10 K to 300 K. Micromagnetic simulations can reproduce these experimental results and give insight into the detailed spin configurations. Furthermore, the simulations are used to map the switching modes of a configurable system with a variable YFe<sub>2</sub> layer thickness. We find the generalized switching modes observed for particular DyFe<sub>2</sub>/YFe<sub>2</sub><sup>24,25</sup> and ErFe<sub>2</sub>/YFe<sub>2</sub><sup>26</sup> multilayers: a mode of independent switching of the RE compounds into the applied field direction with exchange spring winding of the YFe<sub>2</sub> compound at LT, a switching mode where the ErFe<sub>2</sub> moments reverse via an intermediate spin flop state at MT, and an YFe<sub>2</sub> dominated switching mode

with an unwinding of the RE compounds against the applied field direction at HT.

Excitingly, the system with two different magnetically hard materials features a competition of the two respective anisotropies with their distinct properties. It becomes manifest for small  $n$  values when the DyFe<sub>2</sub> and ErFe<sub>2</sub> moments mutually attract each other by exchange interaction that is transmitted through the sandwiched YFe<sub>2</sub> layers. This is the coupled switching mode which is not found on a system with only one hard material: the switching states of both ErFe<sub>2</sub> and DyFe<sub>2</sub> compounds are conjointly located in one plane, and it turns out to be the Dy anisotropy that dominates the competition.

Understanding the manifold switching states present in this accurately reproducible and configurable system will hopefully prove valuable in future for the design of new generation magnetic devices.

- 
- <sup>1</sup> T. Ando and T. Nishihara, IEEE Transactions on Magnetics **33**, 2983 (1997).
- <sup>2</sup> R. H. Victora and X. Shen, IEEE Transactions on Magnetics **41**, 2828 (2005).
- <sup>3</sup> D. Süß, T. Schrefl, S. Fähler, M. Kirschner, G. Hrkac, F. Dorfbauer, and J. Fidler, Appl. Phys. Lett. **87**, 012504 (2005).
- <sup>4</sup> D. Süß, T. Schrefl, R. Dittrich, M. Kirschner, F. Dorfbauer, G. Hrkac, and J. Fidler, IEEE Transactions on Magnetics **290-291**, 551 (2005).
- <sup>5</sup> J.-U. Thiele, S. Maat, and E. E. Fullerton, Appl. Phys. Lett. **82**, 2859 (2003).
- <sup>6</sup> D. Niarchos, Sensors and Actuators A **109**, 166 (2003).
- <sup>7</sup> M. R. J. Gibbs, E. W. Hill, and P. J. Wright, J. Phys. D: Appl. Phys. **37**, R237 (2004).
- <sup>8</sup> O. Cugat, J. Delamare, and G. Reyne, IEEE Transactions on Magnetics **39**, 3607 (2003).
- <sup>9</sup> R. Skomski and J. M. D. Coey, Phys. Rev. B **48**, 15812 (1993).
- <sup>10</sup> E. F. Kneller and R. Hawig, IEEE Transactions on Magnetics **27**, 3588 (1991).
- <sup>11</sup> E. E. Fullerton, J. S. Jiang, M. Grimsditch, C. H. Sowers, and S. D. Bader, Phys. Rev. B **58**, 12193 (1998).
- <sup>12</sup> S. I. Kiselev, J. C. Sankey, I. N. Krivorotov, N. C. Emley, R. J. Schoelkopf, R. A. Buhrman, and D. C. Ralph, Nature **425**, 380 (2003).
- <sup>13</sup> H. Xi, K. Z. Gao, and Y. Shi, IEE Proc.-Circuits Devices Syst. **152**, 301 (2005).
- <sup>14</sup> S. Zhang, P. M. Levy, and A. Fert, Phys. Rev. Lett. **88**, 236601 (2002).
- <sup>15</sup> G. Asti, M. Solzi, M. Ghidini, and F. M. Neri, Phys. Rev. B **69**, 1744011 (2004).
- <sup>16</sup> G. Asti, M. Ghidini, R. Pellicelli, C. Pernechele, M. Solzi, F. Albertini, F. Casoli, S. Fabbri, and L. Pareti, Phys. Rev. B **73**, 0944061 (2006).
- <sup>17</sup> M. Donahue and D. Porter, *Object Oriented Micro-Magnetic Framework (OOMMF)*, [www.nist.gov](http://www.nist.gov).
- <sup>18</sup> *Oxs Extension Module: CED\_UniaxialAnisotropy*, [http://www.soton.ac.uk/fangohr/software/oxs\\_cubic8.html](http://www.soton.ac.uk/fangohr/software/oxs_cubic8.html) (2004).
- <sup>19</sup> A. Mougin, C. Dufour, K. Dumesnil, N. Maloufi, P. Mangin, and G. Patrat, Phys. Rev. B **59**, 5950 (1999).
- <sup>20</sup> K. N. Martin, P. A. J. de Groot, B. D. Rainford, K. Wang, G. J. Bowden, J. P. Zimmermann, and H. Fangohr, Journal of Physics: Condensed Matter **18**, 459 (2006).
- <sup>21</sup> A. Mougin, C. Dufour, K. Dumesnil, and P. Mangin, Phys. Rev. B **62**, 9517 (2000).
- <sup>22</sup> G. J. Bowden, P. A. J. de Groot, B. D. Rainford, K. Wang, K. N. Martin, J. P. Zimmermann, and H. Fangohr, Journal of Physics: Condensed Matter **18**, 5861 (2006).
- <sup>23</sup> A. A. Zhukov, G. J. Bowden, J.-M. L. Beaujour, B. D. Rainford, P. A. J. de Groot, R. C. C. Ward, M. R. Wells, and H. Kämpfer, Journal of Magnetism and Magnetic Materials **270**, 312 (2004).
- <sup>24</sup> K. Dumesnil, M. Dutheil, C. Dufour, and P. Mangin, Phys. Rev. B **62**, 1136 (2000).
- <sup>25</sup> J. P. Zimmermann, K. Martin, G. Bordignon, R. P. Boardman, T. Fischbacher, G. J. Bowden, A. A. Zhukov, H. Fangohr, and P. A. J. de Groot, J. Appl. Phys. **99**, 08B904 (2006).
- <sup>26</sup> K. N. Martin, K. Wang, G. J. Bowden, A. A. Zhukov, P. A. J. de Groot, J. P. Zimmermann, H. Fangohr, and R. C. C. Ward, Journal of Physics: Condensed Matter **89**, 132511 (2006).
- <sup>27</sup> W. F. Brown, Jr., *Micromagnetics* (Wiley Interscience, New York, 1963).
- <sup>28</sup> A. Aharoni, Rev. Mod. Phys. **34**, 227 (1962).
- <sup>29</sup> A. Hubert and R. Schäfer, *Magnetic Domains* (Springer - Verlag Berlin Heidelberg, 1998, 2000).